TITLE

Plasticity and environmental heterogeneity predict geographic resilience patterns of foundation species to future change

AUTHORS

Luca Telesca,[1,2*] Lloyd S. Peck,[2] Trystan Sanders,[3] Jakob Thyrring,[4,5] Mikael K. Sejr,[4,5] Elizabeth M. Harper[1*]

AFFILIATIONS

[1] Department of Earth Sciences, University of Cambridge, CB2 3EQ Cambridge, UK.

[2] British Antarctic Survey, CB3 0ET Cambridge, UK.

[3] GEOMAR Helmholtz Centre for Ocean Research, 24105 Kiel, Germany.

[4] Department of Bioscience, Arctic Research Centre, Aarhus University, 8000 Aarhus C, Denmark.

[5] Department of Bioscience, Marine Ecology, Aarhus University, 8600 Silkeborg, Denmark.

[*] Corresponding authors: Luca Telesca, email: lt401@cam.ac.uk; Elizabeth M. Harper, email: emh21@cam.ac.uk

ABSTRACT

Although geographic patterns of species' sensitivity to global environmental changes are defined by interacting multiple stressors, little is known about the biological mechanisms shaping regional differences in organismal vulnerability. Here, we examine large-scale spatial variations in biomineralisation under heterogeneous environmental gradients of temperature, salinity and food availability across a 30° latitudinal range (3,334 km), to test whether plasticity in calcareous shell production and composition, from juveniles to large adults, mediates geographic patterns of resilience to climate change in critical foundation species, the mussels *Mytilus edulis* and *M. trossulus*. We find mussels produced thinner shells with a higher organic content in polar than temperature regions, indicating decreasing shell calcification towards high latitudes. Salinity was the major driver of regional differences in mussel shell deposition, and in shell mineral and organic composition. In low-salinity environments, the production of calcite and organic shell layers was increased, providing higher resistance against dissolution in more corrosive waters. Conversely, under higher-salinity regimes, increased aragonite deposition suggests enhanced mechanical protection from predators. Interacting strong effects of decreasing salinity and increasing food availability on the compositional shell plasticity in polar and subpolar mussels during growth predict the deposition of a thicker external organic layer (periostracum) under forecasted future environmental conditions. This marked response potential of *Mytilus* species suggests a capacity for increased protection of high-latitude mussel populations from ocean acidification. Our work illustrates that mechanisms driving plastic responses to the spatial structure of multiple stressors can define geographic patterns of unforeseen species resilience to global environmental change.

INTRODUCTION

Unprecedented global environmental changes are driving scientists towards increased understanding of the mechanisms underlying geographic variation in species' responses to future environmental conditions (*1*, *2*). However, our ability to forecast emergent ecological consequences of climate change on marine populations, communities and ecosystems remains limited (*3*). Ecosystem-wide projections are severely constrained by heterogeneous patterns of ocean warming and acidification (*4*), multiple interacting stressors (*5*), and species-specific effects (*6*), as well as predictive models which often exclude important biological mechanisms when projecting changes to species and ecosystems in response to climate change (*2*). A better mechanistic understanding of the biological processes and environmental sources mediating species' responses to disturbances is critical for building the theoretical baseline necessary to forecast the combined effects of multiple emerging stressors (*2*, *3*).

Advances in macroecology suggest that permanent environmental mosaics, defined by spatial overlaps of non-monotonic environmental gradients (*7*), as well as regional adaption or acclimatization (*8–10*), dictate geographic variations in species performance and sensitivity to environmental change in marine ecosystems. Key to these works is that responses vary among populations and individual taxa (*6*, *8*), which often play disproportionately strong roles in structuring benthic communities (*11*). Thus, species-specific biological mechanisms driving organismal variability may shape differential regional responses of foundation species to co-occurring multiple drivers. This can establish spatial patterns of unexpected susceptibility of marine communities to future conditions.

Climate change is considered a major threat to marine ecosystems worldwide, with ocean warming and acidification profoundly affecting species life history and ecology (*6*, *10*), as well as

community structure and ecosystem dynamics (*11*, *12*). Species producing calcium carbonate ($CaCO_3$) shells and skeletons are possibly experiencing the strongest impacts of rapid environmental changes (*6*). Knowledge on their sensitivity is derived largely from experimentally induced responses in model organisms (*1*, *6*), while complex variations under multiple stressors have rarely been investigated in natural environments (*7*, *11–13*). Therefore, inferences made from experimental studies can be misleading and not fully applicable to marine ecosystems (*9*). Indeed, species-specific mechanistic responses to habitat alterations (*14*) on top of mixed outcomes of environmental interactions (additive, synergistic or antagonistic) make future ecosystem predictions extremely challenging. This leaves open the question: do differences in biological mechanisms, shaping regional calcifiers' responses to interacting environmental stressors, define geographic patterns of unforeseen species sensitivity or resilience to global environmental change? A body of research has focused on responses of marine calcifiers to altered water chemistry (*1*, *6*), but studies have rarely considered changes in biogeochemical cycles that strongly mediate biological responses to environmental alterations (*4*). Among those, a marked intensification of the global water cycle in response to warming (+4% for +0.5°C) has been documented over recent decades through changes in ocean salinity (*15*). Salinity is a major ecological factor dictating survival of aquatic organisms and ecosystem functioning. Multidecadal studies have revealed a global salinity pattern following the "rich-get-richer" mechanism, where salty ocean regions (compared to the global mean) are getting saltier (mid-latitudes), whereas low salinity regions are getting fresher (tropical convergence zones and polar regions) (*15*). In a future 2-3°C warmer world (*16*), a substantial 16-24% intensification of the global water cycle is predicted to occur making salinity gradients much sharper (*15*). However, emergent ecological effects of changing salinity on calcifying species and marine communities are largely unknown.

Atlantic mussels, *Mytilus edulis* and *M. trossulus*, are important bed-forming foundation species throughout the eulittoral ecosystems of the northern hemisphere (up to 90% of epibenthic biomass), and represent valuable resources for aquaculture (192,000 t produced in 2015 worth 325 million USD) (*17*). Growing awareness of the consequences of climate change on biodiversity and industry that *Mytilus* species support have stimulated a number of studies to estimate the response potential of these habitat-forming calcifiers to changing ocean conditions (*18–20*).

Calcareous shells perform a range of vital functions including structural support and protection against predators. Because shell integrity determines survival, shell traits are subject to strong selection pressure with functional success or failure a fundamental evolutionary driver. *Mytilus* shell consists of three layers (Fig. 1A-B): (1) the outer organic periostracum, (2) the calcified prismatic and (3) nacreous layers. The periostracum provides the substrate and a protected environment for shell secretion, and is made of sclerotized proteins, protecting shells from corrosive, acidic waters as well as predatory and endolithic borers (*21*). The prismatic and nacreous layers are composed of different mineral forms of $CaCO_3$, calcite and aragonite respectively, dispersed in an organic matrix (*22*). These calcareous layers are characterized by different microstructures and more (e.g. aragonite) or less (e.g. calcite and organics) soluble components the combination of which determines chemical and mechanical shell properties (*23*). Differences in energetic costs of making shell components (*13*) combined with future shifts in environmental gradients (*4*) may influence variations in shell production, composition and structure, shaping regional patterns of shell strength and resistance to acidification.

Mytilus growth, biomineralisation and fitness are linked to multiple drivers, including water temperature, salinity and food supply [chlorophyll-*a* (Chl-*a*) concentration] (*24*, *25*). In the North Atlantic and Arctic Oceans, these key environmental factors vary heterogeneously with latitude

(Fig. 1C-D), encompassing a range of conditions predicted under different future climate change scenarios (*16*). Here we hypothesize that biological mechanisms driving spatial variations in shell production, mineral and organic composition: **i**) shape regional differences in the responses of *Mytilus* species to interacting environmental drivers, and **ii**) define geographic patterns of unanticipated mussel vulnerability in the face of global environmental changes.

Despite projected environmental alterations (*4*, *15*), salinity gradients have been overlooked in large-scale models predicting emergent effects of climate changes on marine organisms. This knowledge is essential to predict whether environmental changes affect shell variability (i.e. thickness, mineral and organic content) and its properties, especially in calcifying foundation species such as *M. edulis* and *M. trossulus*. These factors are crucial for understanding species susceptibility to other rapidly emergent stressors, such as warming and acidification (*3*).

In this study, we examine the relationships between the plasticity in *Mytilus* shell production and composition (from juveniles to large adults) and interactive environmental gradients of temperature, salinity and Chl-*a* concentration in 17 populations spanning a latitudinal range of 30° (3,334 km) across the Atlantic-European and Arctic coastline (Fig. 1C-D). In particular, we test for a latitudinal effect on *Mytilus* shell calcification (variation in shell thickness and organic content) that we hypothesize will show a general decrease from temperate to polar regions. We also identified environmental sources and magnitude of regional variations in shell deposition, to test whether salinity affects shell production and mineral composition during growth, driving changes of mechanical and chemical shell properties. Finally, we modelled spatial trends in the production of individual shell layers with environmental gradients, to test whether biological mechanisms, driving variations in shell structure and properties, shape regional responses of

Mytilus to interacting stressors (especially salinity) and define geographic patterns of sensitivity to future changes.

RESULTS

Generalized linear (mixed) models, GL(M)Ms, were used to explain shell thickness and composition, from juveniles to large adults, with respect to latitude and environmental drivers, and to compare between the individual shell layers.

Latitudinal patterns of shell deposition

GLMMs indicated a general decrease of *Mytilus* whole-shell thickness with increasing latitude from warm-temperate to polar regions (Fig. 2A). We detected a significant negative relationship between the prismatic layer thickness and latitude (Fig. 2A), while no variation in nacreous thickness, periostracum thickness and relative proportion of prismatic layer thickness (calcite%) was found (table S1). Shell length was positively correlated with thickness in all layers indicating thickening during growth (table S1).

The weight proportion (wt%) of organic content in the prismatic layer was modelled with a GLM as a function of collection site and shell thickness. Prismatic layers were characterized by a significantly higher organic content (lower proportion of $CaCO_3$) in mussel shells from polar than temperate regions, indicating decreased shell calcification at higher latitudes (Fig. 2B). Polar shells [sites 15, 16; mean (SD) = 1.8 wt% (0.31)] were characterized by an average of 29% more organic content compared to temperate mussels [sites 1, 11; mean (SD) = 1.4 wt% (0.16)]. The organics wt% was negatively correlated with prismatic thickness (Fig. 2C), indicating a lower proportion of $CaCO_3$ and thinner, so less calcified, shells at polar latitudes.

151 **Environmental influence on shell production and composition**

152 Individual GLMMs were fitted to explain spatial variations in the whole-shell thickness,
153 periostracum thickness and calcite% with environmental gradients during shell growth. We
154 identified significant trends in shell thickness with environmental gradients depending on the shell
155 measurement considered (Fig. 3A-E, fig. S1, Table 1). Whole-shell thickness was positively
156 related to temperature, salinity and shell length, but there was no influence of Chl-*a* (cR^2 = 0.93;
157 Fig. 3A). Salinity had an effect on shell thickness that was 3.4 and 2.1 times larger than temperature
158 and length, respectively (Fig. 3A, Table 1). We detected a negative relationship between calcite%
159 and salinity (95% CI = -12.03 to -2.38, cR^2 = 0.56) (Fig. 3B, table S2), with none of the other
160 drivers having a significant effect.

161 Prismatic and nacreous layers thickness were analysed within the same GLMM. After model
162 selection, fixed continuous covariates of the optimal model, equation (1), were the standardised
163 *temperature*, *salinity*, *Chl-a* concentration and shell *length* in addition to shell *layer* (categorical,
164 two levels: prismatic and nacreous) and their interactions. The random component was the
165 collection *site* used as a random intercept. The model was of the form:

166
$$\begin{aligned} \ln(Thickness_{ijk}) &\sim N(\mu_{ijk};\sigma_j^2) \\ \mu_{ijk} &= Temperature_{ik} + Salinity_{ik} + Chl\text{-}a_{ik} + Length_{ik} + Layer_j \\ &\quad + Temperature_{ik} \times Layer_j + Length_{ik} \times Layer_j + Site_{ij} \\ Site_{ij} &\sim N(0;\sigma_{Site}^2) \end{aligned} \qquad (1)$$

167 where $Thickness_{ijk}$ is the *k*th thickness observation from layer *j* (*j* = prismatic, nacreous) and site *i*
168 (*i* = 1,…, 17). $Site_{ij}$ is the random intercept for layer *j*, which is assumed to be normally distributed
169 with mean 0 and variance σ_{Site}^2.

Sea surface temperature, salinity and shell length all successfully predicted ($cR^2 = 0.93$) variations in the thickness of prismatic and nacreous layers, while no influence of Chl-*a* was detected (Table 1). The mean effect size of salinity on the response was twice as large as the effect of shell length, while it was 2.9 and 4.7 times larger than the effect of temperature on the prismatic and nacreous layers, respectively (equation (2), Fig. 3C-D). This indicates salinity had a stronger contribution to predicting shell structure than the effects of temperature, Chl-*a* and shell length combined (Fig. 4).

$$\mu_{ijk} = \begin{cases} 5.907 + 0.138 \times Temperature + 0.396 \times Salinity + 0.028 \times Chl\text{-}a + 0.197 \times Length & \text{Prismatic} \\ 5.853 + 0.138 \times Temperature + 0.654 \times Salinity + 0.028 \times Chl\text{-}a + 0.308 \times Length & \text{Nacreous} \end{cases} \quad (2)$$

Interactions between shell layer and both salinity and shell length (equation (2)) indicate deposition of proportionally thicker prismatic layers under low salinities and proportionally thicker nacreous layers under higher salinities across the entire range of shell lengths (Fig. 4).

Periostracum plasticity

Models of periostracum thickness revealed significant exponential relationships with Chl-*a* and shell length ($cR^2 = 0.81$) (Table 1). Length had a mean effect that was 3 times larger than Chl-*a* (Fig. 3E), showing a rapid thickening of the periostracum during shell growth. The interactions between shell length and both salinity and temperature indicate that the effects of these variables on periostracum were interdependent. At low salinities, the higher values of shell length had a greater positive effect on periostracum thickness, while the reverse was true for higher temperatures having a marginal effect only on thickening rates (Fig. 5A-B). This suggests that increasing shell size was a more important factor for periostracum growth in fresher waters than in relatively saltier conditions.

192

193 **Among-site shell variation**

194 GLMMs showed no difference in collection site-level effects (conditional modes) on each
195 thickness measurement (Fig. 5C). This indicated no residual effect of species identity or
196 hybridization on the thickness of individual shell layers at different sites after accounting for the
197 effects of environmental factors and shell length.

198

199 **DISCUSSION**

200 Our results demonstrate that plasticity in shell production in *Mytilus* species and the spatial
201 structure of environmental conditions drive geographic variations in shell responses shaping
202 regional differences in the resilience of these foundation species to global environmental change.
203 An understanding of the biological mechanisms driving regional species' responses to multiple
204 interacting stressors is crucial for improving predictive accuracy and informing more realistic
205 projections of species and ecosystem resilience to climate change (*2*). Heterogeneous population-
206 level responses from different climates suggest that environmental stressors, especially salinity,
207 drive regional variations in *Mytilus* shell production, mineral (prismatic and nacreous) and organic
208 (periostracum) composition during growth, which is reflected in the relative proportion of each
209 shell layer. Variations in shell production and composition determine geographic differences in
210 chemical and mechanical protection of shells, shaping the vulnerability of these habitat-forming
211 species to future conditions.

212 Decreasing shell calcification (increasing organic content and thinner shells) towards high latitudes
213 (Fig. 2) supports documented patterns of skeletal production (*13*, *26*). Two explanatory paradigms
214 exist for decreased skeletal size at higher latitudes: increased calcification costs (*13*) and reduced

predation pressure (*27*). Given the higher production cost of organics than $CaCO_3$ deposition (*13*) and problematic protein production at polar temperatures (*28*), we might expect a reduced proportion of organic matrix. Moreover, decreasing predation pressure (*27*) should result in thinner shells of the same composition irrespective of geographic area. However, the wt% of organic matrix was higher at Arctic latitudes. This could suggest either (or a combination of) a marked increase in the cost of calcification in polar regions (*13*), altering significantly the relative costs of $CaCO_3$ and organics production, or a decreased saturation state (increased dissolution) of $CaCO_3$ due to low temperatures and, more importantly, salinity (low $[Ca^{2+}]$ availability) (*25*). In either case, these underlying effects would result in decreased shell calcification at high latitudes. This increased proportion of organic matrix could protect the calcified shell components from dissolution and have an adaptive beneficial effect in more corrosive conditions.

Our results illustrate that different drivers significantly affect both shell thickness and composition in *Mytilus* (Fig. 3). For over 60 years, temperature and shell size have been considered key drivers of $CaCO_3$ shell mineralogy across latitudes, dictating the formation of predominantly aragonitic structures in temperate regions and increased calcite precipitation in cold climates (*29–31*). Although our study partly supports previous findings, we demonstrate that salinity has the strongest influence on shell production and composition in *Mytilus*, which is contrary to the general assumption of temperature and shell size being the primary drivers of shell compositional plasticity.

The interaction between shell layer, salinity and shell size indicates heterogeneous, age-related compositional changes in *Mytilus* shells across different salinities (Fig. 4A). Shifts in shell properties from juveniles to large adults are strongly modulated by salinity, which leads to the formation of exclusively prismatic-dominated shells in brackish waters and nacreous-dominated

structures under marine conditions (Fig. 4B). These patterns, which we show were independent of species or hybrid status (Fig. 5C), indicate that mussel shell plasticity during growth (the *Length* × *Layer* interaction, equation (1)) has an indirect effect on layer thickness by allowing salinity-induced compositional changes and, therefore, the production of the most appropriate shell structure for specific environmental conditions.

Under current scenarios, plasticity in shell production could confer *Mytilus* species an advantage when facing different water chemistries and predation levels. In fact, at high-latitudes and in the Baltic region, where durophagous (shell-breaking) predators are rare or absent and the water is more corrosive (*13*, *27*), mussels are characterized by thinner, prismatic-dominated shells, providing a generally higher protection from dissolution. Conversely, at mid-latitudes, where durophagous predators are more abundant and the $CaCO_3$ solubility of the water is lower (*13*), mussels display thicker, nacreous-dominated shells with higher mechanical resistance.

Despite rapid global changes in the water cycle and salinity gradients (*15*), *Mytilus* species shows a strong capacity to respond to heterogeneous environments. This plasticity in shell production could help to mitigate the emergent negative effects of changing water chemistry. In fact, the interacting effects of salinity and shell length, as well as a minor influence of temperature, on the periostracum (Fig. 5A-B), which represents a strong chemical barrier to dissolution in molluscs (*21*, *32*, *33*), suggest enhanced periostracal thickness under decreasing salinities could mediate impacts of ocean acidification.

Although populations in high-latitude ecosystems will experience globally the most rapid acidification (*4*), the concurrent decrease in salinity predicts thicker prismatic layers and periostraca will be produced which increase protection from higher solubility conditions.

Conversely, in temperate areas, increasing salinity would determine deposition of thicker shells and a relatively thicker nacreous layer and thinner periostracum, favouring mechanical shell resistance. However, predicted changes in periostracal thickening rate under different salinities depend on shell size and would be more evident in larger individuals (length > 48 mm) (Fig. 5A).

In Greenland, where the rate of melting of the ice sheet has doubled in the last decade (*34*), low salinities during summer (< 20 psu) and high productivity (food supply) in coastal areas and fjords (*35*) predict formation of thicker periostraca and increased relative thickness of organic-enriched (high wt%) calcitic layers. These changes could make Arctic *Mytilus* populations more resilient to future acidification. Differently, in the Baltic Sea, the forecasted decrease in salinity (maximum 45% reduction) (*36*), combined with a considerable physiological stress, would be particularly critical for mussels inhabiting already unfavourable conditions for calcification (salinity from 22 psu to 3 psu, low water [Ca^{2+}], and $CaCO_3$ saturation state) (*25*). Moreover, the reduced shell size of Baltic *Mytilus* does not predict formation of thicker periostraca, which would further increase vulnerability to dissolution. Impacts of changing salinity on this habitat-forming species, which contributes up to 90% of the Baltic benthic biomass, could strongly affect the ecosystem, most likely resulting in substantial range restrictions towards higher salinity areas.

Although our results strongly support the hypothesis that biological mechanisms for variations in shell production can shape regional responses in *Mytilus*, changes of other biological drivers, such as predation pressure and primary production, could also have profound influences (*13*, *37*). In fact, as temperature rises, durophagous predators could expand their ranges towards polar regions (*38*), suggesting an increased vulnerability of thin-shelled individuals. However, predicted northward phytoplankton expansions and an overall increase in primary production at high

latitudes (*37*), could favour periostracal growth potential in *Mytilus* and, thus, increased resistance to dissolution for all the size classes in polar and subpolar regions.

Mytilus shells have a thick periostracum and a marked compositional plasticity compared to other calcifiers that often compete with it for space (e.g. barnacles and spirorbid polychaetes). This layer provides a strong defence against shell dissolution allowing mytilids to survive in oligohaline waters (~5 psu) and extremely acidified conditions (e.g. hydrothermal vents) (*33*). These factors may shift the ecological balance and community structure in favour of species with stronger resistance to corrosive conditions, such as mussels, when ocean waters become fresher and more acidic in future decades.

As hypothesised, plasticity in shell production and the spatial structure of environmental conditions drive regional differences in *Mytilus* shell deposition and composition, shaping spatial patterns of chemical and mechanical shell properties. Overall, mussel shell calcification decreased towards high latitudes, with salinity being the major driver of geographical variations in shell production, mineral and organic composition. The marked compositional plasticity in calcareous shell components (prismatics and nacreous layers) suggest an higher resistance against dissolution for mussels in polar, low-salinity environments, and an enhanced mechanical shell protection from predators in temperate, higher-salinity regions. The strong response potential of *Mytilus* shell periostracum to heterogeneous environments predicts an increased resilience to ocean acidification in polar and sub-polar mussels, and a higher sensitivity of Baltic populations under future environmental conditions.

In conclusion, our findings demonstrate that biological mechanisms, driving spatial variability of mussel responses to interacting environmental factors, shape the complex geographic pattern of

shell deposition and properties, dictating regional differences in *Mytilus* species sensitivity to future environmental change. As the magnitude of anthropogenic impacts continue to increase, further studies are need to better understand the key biological processes mediating species' response to habitat alterations, especially for those having both high climate sensitivity and disproportionately strong ecological impacts in shaping marine communities. This knowledge underpins our ability to predict accurately and reduce the damaging effect of climate change on future biodiversity under any range of scenarios (*2*). Our study has important implications because it clarifies the links between (**i**) the mechanisms of biological variation, (**ii**) the predicted shift in spatial co-occurrence of multiple environmental drivers, and (**iii**) regional differences in the plastic responses and sensitivity of calcifying, foundation species to changing habitats. This understanding is of critical importance for making realistic projections of emergent ecological effects of global environmental changes, such as altered salinity regimes, and to improve our predictive accuracy for impacts on marine communities and ecosystems, and the services they provide.

MATERIALS AND METHODS

Mytilus collection

We sampled individuals from a total of 17 *Mytilus* (*Mytilus edulis* and *M. trossulus*) populations along the North Atlantic, Arctic and Baltic Sea coastlines from four distinctive climatic regions (warm-temperate, cold-temperate, subpolar and polar) covering a latitudinal range of 30° (a distance of 3,334 km), from Western European (Brest, North-West France, 48°N) to Northern Greenlandic (Qaanaaq, North-West Greenland 78°N) coastlines (Fig. 1C). During December 2014 - September 2015, mussels of various size classes for each site (shell length 26-81 mm) were

sampled from the eulittoral zone on rocky shores for a total of 424 individuals (table S3). For each specimen, shell length was measured with digital calipers (0.01 mm precision) and used as a within-population proxy for age.

We analysed *Mytilus* populations of which the genetic structure was known, with particular focus on species identity and hybrid status (*M. edulis* × *M. trossulus*). *Mytilus* shells used were either from specimens already evaluated in genetic investigations or mussels obtained from sites routinely used in regional monitoring programs that provided information on species identity (table S3). Areas where the Mediterranean mussel, *Mytilus galloprovincialis*, was present were avoided. We did, however, sample few sites with very low levels of *M. edulis* × *M. galloprovincialis* hybridization.

Mussel shell preparation

We set left shell valves in polyester resin (Kleer-Set FF, MetPrep, Coventry, U.K.) blocks. Embedded specimens were sliced longitudinally along their axis of maximum growth (Fig. 1A) using a diamond saw and then progressively polished with silicon carbide paper (grit size: P800-P2500) and diamond paste (grading: 9-1 µm). Photographs of polished sections (Fig. 1B) were acquired with a stereo-microscope (Leica M165 C equipped with a DFC295 HD camera, Leica, Wetzlar, Germany) and shell thickness (µm) was measured using the Fiji software (v1.51u). Since larger individuals had undergone evident environmental abrasion or dissolution which removed the periostracum and prismatic layer closer to the umbo, we estimated the thickness of the whole-shell, prismatic and nacreous layers at the midpoint along the shell cross-section. The proportion of calcite was estimated as

$$\text{calcite\%} = (\text{prismatic thickness} / \text{whole-shell thickness}) \times 100$$

Periostracum thickness was measured at the posterior edge where it attaches to the external side of the prismatic layer, to estimate the fully formed organic layer that was unaffected by decay or abrasion (*21*).

Organic content analyses

We performed thermogravimetric analyses (TGA) to estimate the weight proportion (wt%) of organic matrix within the prismatic layer. *Mytilus edulis* specimens were selected from four populations (sites 1, 11, 15, 16) to explore differences in shell organic content under temperate and polar regimes. We removed the periostracum by sanding, and prismatic layer tiles (8 × 5 mm, $N = 20 \times 4$ sites) were isolated along the posteroventral shell margin. Tiles were cleaned, air-dried and then finely ground. We tested ten milligrams of this powdered shell with a thermogravimetric analyser (TGA Q500, TA Instruments, New Castle, DE, U.S.A.). Samples were subjected to constant heating from ~25°C to 700°C at a linear rate of 10°C min^{-1} under a dynamic nitrogen atmosphere and weight changes were recorded (Supplementary Material and Methods). We estimated the wt% of organic matter within the shell microstructure as the proportion of weight loss during the thermal treatment between 150°C and 550°C (fig. S2).

Environmental characterization

We selected three key environmental drivers based on their known influence on mussel growth, their level of collinearity across the geographic scale investigated and the forecasted major ocean alterations under climate change (*16*). For each site, measurements of sea surface temperature, salinity and Chl-*a* concentration, the latter being used as a proxy for food supply (*24*), were generated using the Copernicus Marine Environment Monitoring Service (CMEMS)

(http://marine.copernicus.eu/). These climate datasets are composed of high-resolution physical and biogeochemical assimilated (integration of observational and predicted information) daily data (N = 2,191 per parameter) (see data file S1). To provide a first order approximation of the water conditions prevailing during the near-maximum rates of shell deposition (*30*), we expressed parameters as mean May-October values averaged over the 6-year period 2009-2014 and used these as input variables (Fig. 1D, table S4).

Direct environmental monitoring for each site was not feasible due to the number of populations analysed, their geographic range (> 3,300 km) and the temporal resolution (6 years) required to estimate the average growth conditions during the lifespan of sampled specimens. For this large-scale study, remote-sensing and assimilated data presented potential advantages compared to traditional measurements due to their high spatio-temporal resolution, advanced calibration and validation (i.e. high correlation with discrete field measurements).

Statistical analysis

GLMMs were applied to account for the hierarchical structure of the dataset consisting of multiple specimens (N = 24-26 replicates) from each collection site and to generalize our results to *Mytilus* populations beyond the study sample.

We carried out data exploration following the protocol of Zuur *et al.* (*39*). Initial inspection revealed no outliers. Pairwise scatterplots and variance inflation factors (VIFs) were calculated to check for collinearity between input variables. VIF values < 2 indicated an acceptable degree of correlation among covariates to be included within the same model. We applied residual regression to uncouple the unique from the shared contribution of temperature and Chl-*a* concentration to the response (*40*). This allowed us to account for the existing causal link between these two parameters

and to avoid inferential problems from modelling non-independent covariates without losing explanatory power (*40*). To directly compare model estimates from predictors on different measurement scales, estimate biologically meaningful intercepts and interpret main effects when interactions are present, we standardised all the input variables (environmental parameters and shell length). For standardisation, we subtracted the sample mean from the variable values and divided them by the sample standard deviation $[z_i = (x_i - \bar{x})/\sigma_x]$. Preliminary inspection of residual patterns showed heteroscedasticity in most models. The use of different continuous probability distributions (i.e. gamma) and link functions did not stabilize the variance, therefore a ln-transformation of the response was required, except for calcite% and wt% measurements. Response variables did not require further transformations.

We used separate GLMMs to explore patterns of shell thickness of individual layers with latitude and shell length (size). The proportion (wt%) of organic matrix ($N = 80$) was modelled as a function of site (categorical, four levels) and prismatic thickness (continuous) to test for differences between polar and temperate regions and association with shell thickness. The response variable was coded as a value from 0 to 1; therefore, we used a GLM with a beta distribution and a logistic link function. Pair-wise contrasts with a Bonferroni correction were then used to test for differences in wt% among sites within and between climatic regions.

Different approaches were used to investigate the relationships between shell thickness and environmental gradients. Whole-shell thickness, periostracum thickness and calcite% were modelled separately ($N = 424$ each). Prismatic and nacreous layer thickness were analysed within the same GLMM, allowing the simultaneous prediction of common and divergent environmental effects on both layers and to reduce the probability of type I error. To model shell thickness ($N =$

418 424 × 2 layers) as a function of the environmental predictors we used a GLMM with a normal
419 distribution (equation (1)). In the initial model, fixed continuous covariates were the standardised
420 temperature, salinity and Chl-*a* in addition to shell layer (categorical, two levels) and their two-
421 way interactions. Shell length (continuous) was included to control for possible effects of within
422 population age on layer thickness. To incorporate the dependency among observations for a
423 specific layer from the same collection site, we used site as a random intercept.

424 Models were optimized by first selecting the random structure and then the optimal fixed
425 component. The principal tools for model comparison were the corrected Akaike Information
426 Criterion (AICc) and bootstrapped likelihood ratio tests. Random terms were selected on prior
427 knowledge of the dependency structure of the dataset. Visual inspection of residual patterns
428 indicated violation of homogeneity in most cases. This required the use of variance structures
429 (generalized least squares) allowing the residual spread to vary with respect to shell layer. The
430 fixed component was optimized by rejecting only non-significant interaction terms that minimized
431 the AICc value. For all model comparisons, variation of AICc between the optimal (lowest AICc
432 value) and competing models were greater than 8, and fixed-effect estimates were nearly identical,
433 indicating that competing models were very unlikely to be superior (*41*). The proportion of
434 variance explained by the models was quantified with conditional or pseudo determination
435 coefficients (cR^2 or $pseudoR^2$). We used variograms to assess the absence of spatial
436 autocorrelation. Final models were validated by inspection of standardised residual patterns to
437 verify GLMM assumptions of normality, homogeneity and independence. We used optimal
438 models to estimate the mean effect sizes (same measurement scale) of environmental drivers on
439 the response. Ninety-five per cent confidence intervals (95% CI) for the regression parameters
440 were generated using bias-corrected parametric bootstrap methods (10,000 iterations). 95% CIs

were used for statistical inference due to estimation of approximated significance values (*P*-value) in mixed-modelling. If the confidence intervals did not overlap zero, then the effect was considered significant. All data exploration and statistical analyses were performed in R (v3.4.1) (for packages see table S5).

REFERENCES

1. I. Nagelkerken, S. D. Connell, Global alteration of ocean ecosystem functioning due to increasing human CO_2 emissions. *Proc. Natl. Acad. Sci. U.S.A.* **112**, 13272–13277 (2015).
2. M. C. Urban, G. Bocedi, A. P. Hendry, J.-B. Mihoub, G. Peer, A. Singer, J. R. Bridle, L. G. Crozier, L. De Meester, W. Godsoe, A. Gonzalez, J. J. Hellmann, R. D. Holt, A. Huth, K. Johst, C. B. Krug, P. W. Leadley, S. C. F. Palmer, J. H. Pantel, A. Schmitz, P. A. Zollner, J. M. J. Travis, Improving the forecast for biodiversity under climate change. *Science*. **353**, aad8466 (2016).
3. K. J. Kroeker, R. L. Kordas, C. D. G. Harley, Embracing interactions in ocean acidification research: confronting multiple stressor scenarios and context dependence. *Biol. Lett.* **13**, 20160802 (2017).
4. J. P. Gattuso, A. Magnan, R. Bille, W. W. L. Cheung, E. L. Howes, F. Joos, D. Allemand, L. Bopp, S. R. Cooley, C. M. Eakin, O. Hoegh-Guldberg, R. P. Kelly, H. O. Portner, A. D. Rogers, J. M. Baxter, D. Laffoley, D. Osborn, A. Rankovic, J. Rochette, U. R. Sumaila, S. Treyer, C. Turley, Contrasting futures for ocean and society from different anthropogenic CO_2 emissions scenarios. *Science*. **349**, aac4722 (2015).
5. D. L. Breitburg, J. Salisbury, J. Bernhard, W.-J. Cai, S. Dupont, S. Doney, K. Kroeker, L. Levin, W. C. Long, L. Milke, S. Miller, B. Phelan, U. Passow, B. Seibel, A. Todgham, A. Tarrant, And

on top of all that… Coping with ocean acidification in the midst of many stressors. *Oceanography*. **28**, 48–61 (2015).

6. K. J. Kroeker, R. L. Kordas, R. Crim, I. E. Hendriks, L. Ramajo, G. S. Singh, C. M. Duarte, J.-P. Gattuso, Impacts of ocean acidification on marine organisms: quantifying sensitivities and interaction with warming. *Glob. Change Biol.* **19**, 1884–1896 (2013).

7. K. J. Kroeker, E. Sanford, J. M. Rose, C. A. Blanchette, F. Chan, F. P. Chavez, B. Gaylord, B. Helmuth, T. M. Hill, G. E. Hofmann, M. A. McManus, B. A. Menge, K. J. Nielsen, P. T. Raimondi, A. D. Russell, L. Washburn, Interacting environmental mosaics drive geographic variation in mussel performance and predation vulnerability. *Ecol. Lett.* **19**, 771–779 (2016).

8. P. Calosi, S. Melatunan, L. M. Turner, Y. Artioli, R. L. Davidson, J. J. Byrne, M. R. Viant, S. Widdicombe, S. D. Rundle, Regional adaptation defines sensitivity to future ocean acidification. *Nat. Commun.* **8**, 13994 (2017).

9. C. A. Vargas, N. A. Lagos, M. A. Lardies, C. Duarte, P. H. Manríquez, V. M. Aguilera, B. Broitman, S. Widdicombe, S. Dupont, Species-specific responses to ocean acidification should account for local adaptation and adaptive plasticity. *Nat. Ecol. Evol.* **1**, 0084 (2017).

10. L. S. Peck, *Oceanogr. Mar. Biol.*, in press.

11. G. V. Ashton, S. A. Morley, D. K. A. Barnes, M. S. Clark, L. S. Peck, Warming by 1°C drives species and assemblage level responses in Antarctica's marine shallows. *Curr. Biol.* **27**, 2698–2705.e3 (2017).

12. L. S. Peck, M. S. Clark, D. Power, J. Reis, F. M. Batista, E. M. Harper, Acidification effects on biofouling communities: winners and losers. *Glob. Change Biol.* **21**, 1907–1913 (2015).

13. S.-A. Watson, S. A. Morley, L. S. Peck, Latitudinal trends in shell production cost from the tropics to the poles. *Sci. Adv.* **3**, e1701362 (2017).

14. M. S. Clark, U. Sommer, J. K. Sihra, M. A. S. Thorne, S. A. Morley, M. King, M. R. Viant, L. S. Peck, Biodiversity in marine invertebrate responses to acute warming revealed by a comparative multi-omics approach. *Glob. Change Biol.* **23**, 318–330 (2017).

15. P. J. Durack, S. E. Wijffels, R. J. Matear, Ocean salinities reveal strong global water cycle intensification during 1950 to 2000. *Science*. **336**, 455–458 (2012).

16. B. Kirtman, S. B. Power, J. A. Adedoyin, G. J. Boer, R. Bojariu, I. Camilloni, F. J. Doblas-Reyes, A. M. Fiore, M. Kimoto, G. A. Meehl, M. Prather, A. Sarr, C. Schär, R. Sutton, G. J. van Oldenborgh, G. Vecchi, H. J. Wang, in *Climate Change 2013: The Physical Science Basis. Contribution of Working Group I to the Fifth Assessment Report of the Intergovernmental Panel on Climate Change*, T. F. Stocker, D. Qin, G.-K. Plattner, M. Tignor, S. K. Allen, J. Boschung, A. Nauels, Y. Xia, V. Bex, P. M. Midgley, Eds. (Cambridge University Press, Cambridge, UK, 2013), pp. 953–1028.

17. FAO, "FAO Yearbook. Fishery and Aquaculture Statistics. 2015" (Rome, 2017), (available at http://www.fao.org/documents/card/en/c/68440a7a-2adb-416d-872b-b233eb44f6c9/).

18. L. Telesca, K. Michalek, T. Sanders, L. S. Peck, J. Thyrring, E. M. Harper, Blue mussel shell shape plasticity and natural environments: a quantitative approach. *Sci. Rep.* **8**, 2865 (2018).

19. J. Thyrring, M. Blicher, J. Sørensen, S. Wegeberg, M. Sejr, Rising air temperatures will increase intertidal mussel abundance in the Arctic. *Mar. Ecol. Prog. Ser.* **584**, 91–104 (2017).

20. J. Thomsen, L. S. Stapp, K. Haynert, H. Schade, M. Danelli, G. Lannig, K. M. Wegner, F. Melzner, Naturally acidified habitat selects for ocean acidification–tolerant mussels. *Sci. Adv.* **3**, e1602411 (2017).

21. E. M. Harper, The molluscan periostracum: an important constraint in bivalve evolution. *Palaeontology*. **40**, 71–97 (1997).

22. A. G. Checa, C. M. Pina, A. J. Osuna-Mascaró, A. B. Rodríguez-Navarro, E. M. Harper, Crystalline organization of the fibrous prismatic calcitic layer of the Mediterranean mussel *Mytilus galloprovincialis*. *Eur. J. Mineral.* **26**, 495–505 (2014).

23. S. C. Fitzer, W. Zhu, K. E. Tanner, V. R. Phoenix, N. A. Kamenos, M. Cusack, Ocean acidification alters the material properties of *Mytilus edulis* shells. *J. R. Soc. Interface*. **12**, 20141227 (2015).

24. J. Thomsen, I. Casties, C. Pansch, A. Körtzinger, F. Melzner, Food availability outweighs ocean acidification effects in juvenile *Mytilus edulis*: laboratory and field experiments. *Glob. Change Biol.* **19**, 1017–1027 (2013).

25. J. Thomsen, K. Ramesh, T. Sanders, M. Bleich, F. Melzner, Calcification in a marginal sea – influence of seawater [Ca^{2+}] and carbonate chemistry on bivalve shell formation. *Biogeosciences*. **15**, 1469–1482 (2018).

26. S.-A. Watson, L. S. Peck, P. A. Tyler, P. C. Southgate, K. S. Tan, R. W. Day, S. A. Morley, Marine invertebrate skeleton size varies with latitude, temperature and carbonate saturation: implications for global change and ocean acidification. *Glob. Change Biol.* **18**, 3026–3038 (2012).

27. E. M. Harper, L. S. Peck, Latitudinal and depth gradients in marine predation pressure. *Glob. Ecol. Biogeogr.* **25**, 670–678 (2016).

28. L. S. Peck, A cold limit to adaptation in the sea. *Trends Ecol. Evol.* **31**, 13–26 (2016).

29. H. A. Lowenstam, Factors affecting the aragonite:calcite ratios in carbonate-secreting marine organisms. *J. Geol.* **62**, 284–322 (1954).

30. J. G. Carter, R. Seed, in *Bivalves: an Eon of Evolution*, P. A. Johnston, J. W. Haggart, Eds. (University of Calgary Press, Vancouver, 1998), pp. 87–117.

533 31. L. Ramajo, A. B. Rodriguez-Navarro, C. M. Duarte, M. A. Lardies, N. A. Lagos, Shifts in shell
534 mineralogy and metabolism of *Concholepas concholepas* juveniles along the Chilean coast. *Mar.*
535 *Freshw. Res.* **66**, 1147 (2015).
536 32. V. L. Peck, G. A. Tarling, C. Manno, E. M. Harper, E. Tynan, Outer organic layer and internal
537 repair mechanism protects pteropod *Limacina helicina* from ocean acidification. *Deep-Sea Res.*
538 *Pt. II*. **127**, 41–52 (2016).
539 33. V. Tunnicliffe, K. T. A. Davies, D. A. Butterfield, R. W. Embley, J. M. Rose, W. W. Chadwick
540 Jr, Survival of mussels in extremely acidic waters on a submarine volcano. *Nat. Geosci.* **2**, 344–
541 348 (2009).
542 34. K. K. Kjeldsen, N. J. Korsgaard, A. A. Bjørk, S. A. Khan, J. E. Box, S. Funder, N. K. Larsen, J.
543 L. Bamber, W. Colgan, M. van den Broeke, M.-L. Siggaard-Andersen, C. Nuth, A. Schomacker,
544 C. S. Andresen, E. Willerslev, K. H. Kjær, Spatial and temporal distribution of mass loss from the
545 Greenland Ice Sheet since AD 1900. *Nature*. **528**, 396–400 (2015).
546 35. L. Meire, J. Mortensen, P. Meire, T. Juul-Pedersen, M. K. Sejr, S. Rysgaard, R. Nygaard, P.
547 Huybrechts, F. J. R. Meysman, Marine-terminating glaciers sustain high productivity in
548 Greenland fjords. *Glob. Change Biol.* **23**, 5344–5357 (2017).
549 36. U. Gräwe, R. Friedland, H. Burchard, The future of the western Baltic Sea: two possible
550 scenarios. *Ocean Dyn.* **63**, 901–921 (2013).
551 37. S. Dutkiewicz, J. J. Morris, M. J. Follows, J. Scott, O. Levitan, S. T. Dyhrman, I. Berman-Frank,
552 Impact of ocean acidification on the structure of future phytoplankton communities. *Nat. Clim.*
553 *Change*. **5**, 1002–1006 (2015).
554 38. J. García Molinos, B. S. Halpern, D. S. Schoeman, C. J. Brown, W. Kiessling, P. J. Moore, J. M.
555 Pandolfi, E. S. Poloczanska, A. J. Richardson, M. T. Burrows, Climate velocity and the future

556 global redistribution of marine biodiversity. *Nat. Clim. Change*. **6**, 83–88 (2016).

557 39. A. F. Zuur, E. N. Ieno, C. S. Elphick, A protocol for data exploration to avoid common statistical
558 problems. *Methods Ecol. Evol.* **1**, 3–14 (2010).

559 40. M. H. Graham, Confronting multicollinearity in ecological multiple regression. *Ecology*. **84**,
560 2809–2815 (2003).

561 41. K. P. Burnham, D. R. Anderson, *Model Selection and Multimodel Inference : a Practical*
562 *Information-Theoretic Approach* (Springer-Verlag, New York, NY, USA, 2002).

563 42. C. M. Zaremba, D. E. Morse, S. Mann, P. K. Hansma, G. D. Stucky, Aragonite−hydroxyapatite
564 conversion in gastropod (Abalone) nacre. *Chem. Mater.* **10**, 3813–3824 (1998).

565 43. T. Kijewski, B. Śmietanka, M. Zbawicka, E. Gosling, H. Hummel, R. Wenne, Distribution of
566 *Mytilus* taxa in European coastal areas as inferred from molecular markers. *J. Sea Res.* **65**, 224–
567 234 (2011).

568 44. N. Bierne, P. Borsa, C. Daguin, D. Jollivet, F. Viard, F. Bonhomme, P. David, Introgression
569 patterns in the mosaic hybrid zone between *Mytilus edulis* and *M. galloprovincialis*. *Mol. Ecol.*
570 **12**, 447–461 (2003).

571 45. T. Hilbish, E. Carson, J. Plante, L. Weaver, M. Gilg, Distribution of *Mytilus edulis*, *M.*
572 *galloprovincialis*, and their hybrids in open-coast populations of mussels in southwestern
573 England. *Mar. Biol.* **140**, 137–142 (2002).

574 46. T. Kijewski, J. W. M. Wijsman, H. Hummel, R. Wenne, Genetic composition of cultured and
575 wild mussels *Mytilus* from The Netherlands and transfers from Ireland and Great Britain.
576 *Aquaculture*. **287**, 292–296 (2009).

577 47. H. Stuckas, L. Knöbel, H. Schade, C. Breusing, H.-H. Hinrichsen, M. Bartel, K. Langguth, F.
578 Melzner, Combining hydrodynamic modelling with genetics: can passive larval drift shape the

579 genetic structure of Baltic *Mytilus* populations? *Mol. Ecol.* **26**, 2765–2782 (2017).

580 48. T. K. Kijewski, M. Zbawicka, R. Väinölä, R. Wenne, Introgression and mitochondrial DNA
581 heteroplasmy in the Baltic populations of mussels *Mytilus trossulus* and *M. edulis*. *Mar. Biol.*
582 **149**, 1371–1385 (2006).

583 49. H. Stuckas, K. Stoof, H. Quesada, R. Tiedemann, Evolutionary implications of discordant clines
584 across the Baltic *Mytilus* hybrid zone (*Mytilus edulis* and *Mytilus trossulus*). *Heredity (Edinb).*
585 **103**, 146–156 (2009).

586 50. C. Breusing, *Population Genetics and Morphometric Variation of Blue Mussels in the Western*
587 *Baltic Sea.* (Master Thesis. GEOMAR Helmholtz Centre for Ocean Research Kiel, 2012;
588 http://oceanrep.geomar.de/19887/).

589 51. R. Väinölä, P. Strelkov, *Mytilus trossulus* in Northern Europe. *Mar. Biol.* **158**, 817–833 (2011).

590 52. T. Yarra, K. Gharbi, M. Blaxter, L. S. Peck, M. S. Clark, Characterization of the mantle
591 transcriptome in bivalves: *Pecten maximus*, *Mytilus edulis* and *Crassostrea gigas*. *Mar. Genom.*
592 **27**, 9–15 (2016).

593 53. H. Tyler-Walters, B. James, M. Carruthers, C. Wilding, O. Durkin, C. Lacey, E. Philpott, L.
594 Adamas, P. D. Chaniotis, P. T. V. Wilkes, R. Seeley, M. Neilly, J. Dargie, O. T. Crawford-Avis,
595 "Descriptions of scottish Priority Marine Features (PMFs). Scottish Natural Heritage
596 commissioned report No. 406." (2016).

597 54. S. J. Brooks, E. Farmen, The distribution of the mussel *Mytilus* species along the Norwegian
598 coast. *J. Shellfish Res.* **32**, 265–270 (2013).

599 55. S. S. Mathiesen, J. Thyrring, J. Hemmer-Hansen, J. Berge, A. Sukhotin, P. Leopold, M. Bekaert,
600 M. K. Sejr, E. E. Nielsen, Genetic diversity and connectivity within *Mytilus* spp. in the subarctic
601 and Arctic. *Evol. Appl.* **10**, 39–55 (2017).

602 56. R Core Team, R: a language and environment for statistical computing. (2017), (available at
603 https://www.r-project.org/).
604 57. F. Cribari-Neto, A. Zeileis, Beta regression in R. *J. Stat. Softw.* **34**, 1–24 (2010).
605 58. J. Fox, S. Weisberg, *An R Companion to Applied Regression* (SAGE Publications, Thousand
606 Oaks, CA, USA, 2011; https://uk.sagepub.com/en-gb/eur/an-r-companion-to-applied-
607 regression/book233899).
608 59. H. Wickham, *Ggplot2 : Elegant Graphics for Data Analysis* (Springer, New York, NY, USA,
609 2016).
610 60. D. Bates, M. Mächler, B. Bolker, S. Walker, Fitting linear mixed-effects models using lme4. *J.*
611 *Stat. Softw.* **67**, 1–48 (2015).
612 61. A. Loy, S. Steele, lmeresampler: bootstrap methods for nested linear mixed-effects models.
613 (2016), (available at https://cran.r-project.org/package=lmeresampler).
614 62. A. Kuznetsova, P. B. Brockhoff, R. H. B. Christensen, lmerTest package: tests in linear mixed
615 effects models. *J. Stat. Softw.* **82**, 1–26 (2017).
616 63. K. Barton, MuMIn: Multi-Model Inference. (2017), (available at https://cran.r-
617 project.org/package=MuMIn).
618 64. J. Pinheiro, D. Bates, *Mixed-Effects Models in S and S-PLUS* (Springer-Verlag, New York, USA,
619 2000), *Statistics and Computing*.
620 65. U. Halekoh, S. Højsgaard, A Kenward-Roger approximation and parametric bootstrap methods
621 for tests in linear mixed models - The R package pbkrtest. *J. Stat. Softw.* **59**, 1–32 (2014).
622 66. F. Scheipl, S. Greven, H. Küchenhoff, Size and power of tests for a zero random effect variance
623 or polynomial regression in additive and linear mixed models. *Comput. Stat. Data Anal.* **52**,
624 3283–3299 (2008).

67. P. J. Haines, *Principles of Thermal Analysis and Calorimetry* (Royal Society of Chemistry, Cambridge, UK, 2002; http://ebook.rsc.org/?DOI=10.1039/9781847551764), *RSC Paperbacks*.

68. S. Gaisford, V. Kett, P. J. Haines, *Principles of Thermal Analysis and Calorimetry: Edition 2* (Royal Society of Chemistry, Cambridge, UK, 2016; http://pubs.rsc.org/en/content/ebook/978-1-78262-051-8#!divbookcontent).

Acknowledgments: We thank Iain Johnston (Scottish Oceans Institute, St. Andrews, UK), Sarah Dashfield (Plymouth Marine Laboratory, Plymouth, UK), Dr. Peter Thor (Norwegian Polar Institute, Tromsø, Norway), Alexander Ventura (University of Gothenburg, Kristineberg, Sweden), Dr. Henk van der Veer and Rob Dekker (Royal Netherlands Institute for Sea Research, Texel, Netherlands) for help with specimens collection, and the Statistics Clinic (University of Cambridge, UK) for statistical advice.

Funding: The work was funded by the European Union Seventh Framework Programme, Marie Curie ITN CAlcium in a Changing Environment (CACHE), under grant agreement n° 605051. JT acknowledges additional financial support from the Danish Council for Independent Research, Individual Post-doctoral Grant n° 7027-0060B.

Author contributions: L.T., L.S.P. and E.M.H. conceived the original project and designed the study; L.T. performed laboratory work and thermogravimetric analysis, generated environmental datasets, performed modelling work and analysed output data; L.T., T.S., J.T. and M.K.S. collected materials; L.T., L.S.P. and E.M.H. wrote the first draft of the manuscript, and all co-authors contributed substantially to revisions.

FIGURES AND TABLES

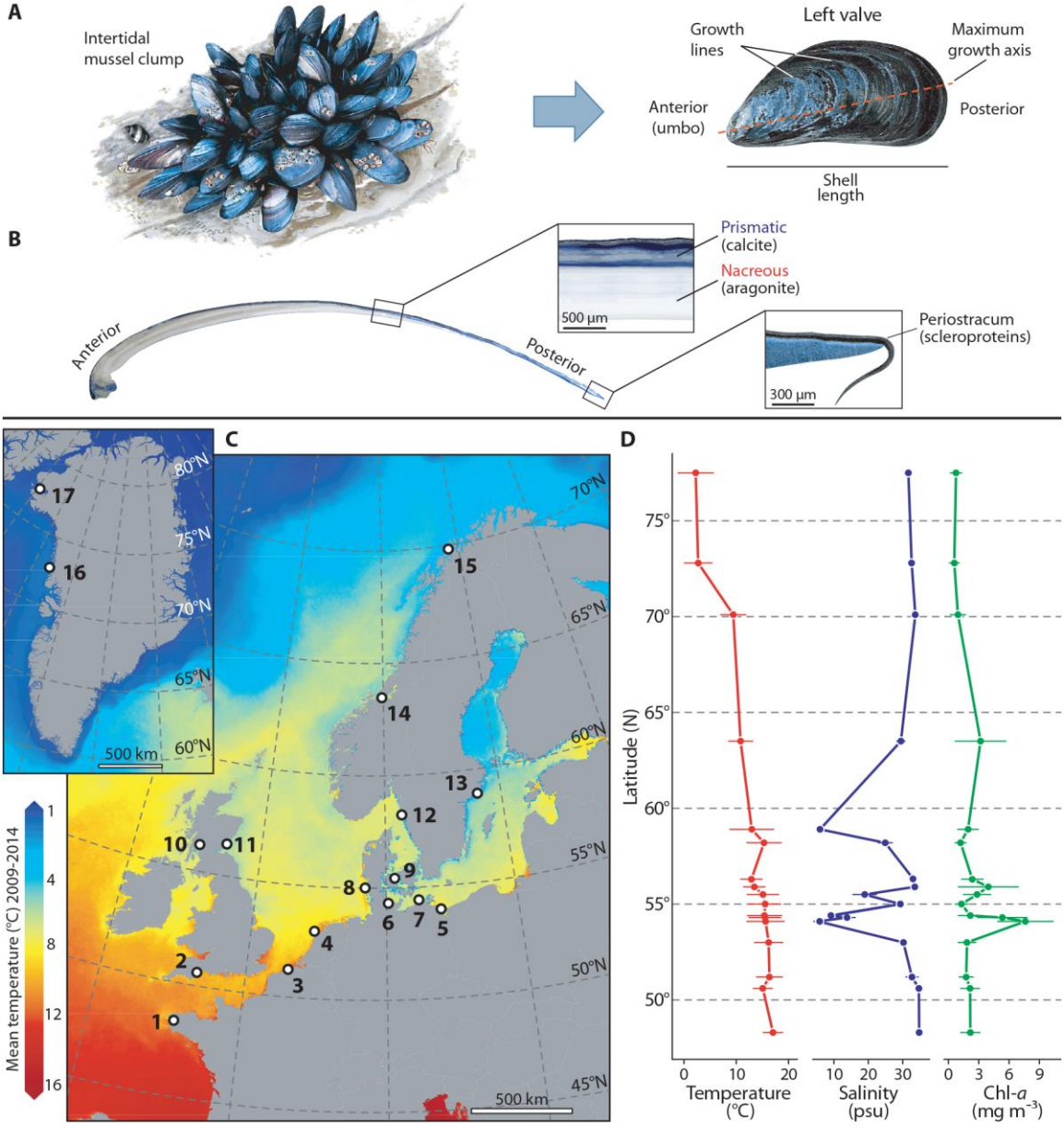

Fig. 1. *Mytilus* spp. shell, collection sites and environmental heterogeneity. (**A**) *Mytilus* shell valve morphology and dimensions. (**B**) Anteroposterior cross-section of shell valve along the axis of maximum growth (from umbo to posterior commissure) showing internal structure and composition of individual mineral (prismatic and nacreous) and organic (periostracum) shell layers. (**C**) Thermal map of North-East Atlantic and Arctic surface

waters from the CMEMS (http://marine.copernicus.eu/) biogeochemical datasets showing locations (open circles) where *Mytilus* was collected from across the Eastern European and Greenlandic coastlines (from 48°N to 78°N): (1) Brest, France, (2) Exmouth, England, (3) Oostende, Belgium, (4) Texel, Netherlands, (5) Usedom, (6) Kiel, (7) Ahrenshoop, (8) Sylt, all Germany, (9) Kerteminde, Denmark, (10) Tarbet, Scotland, (11) St. Andrews, Scotland, (12) Kristineberg, Sweden, (13) Nynäshamn, Sweden (14) Trondhiem, Norway, (15) Tromsø, Norway, (16) Upernavik, Greenland and (17) Qaanaaq, Greenland. Map created with ArcMap 10.5 (ArcGIS software by Esri, http://esri.com), background image courtesy of OpenStreetMap (http://www.openstreetmap.org). (**D**) Latitudinal gradients for sea surface temperature, salinity and chlorophyll-*a* (Chl-*a*) concentration, showing environmental heterogeneity across the study regions. Mean values (May - October, filled circles) and SD (horizontal lines) for the 6-year period 2009 - 2014 were estimated from CMEMS datasets.

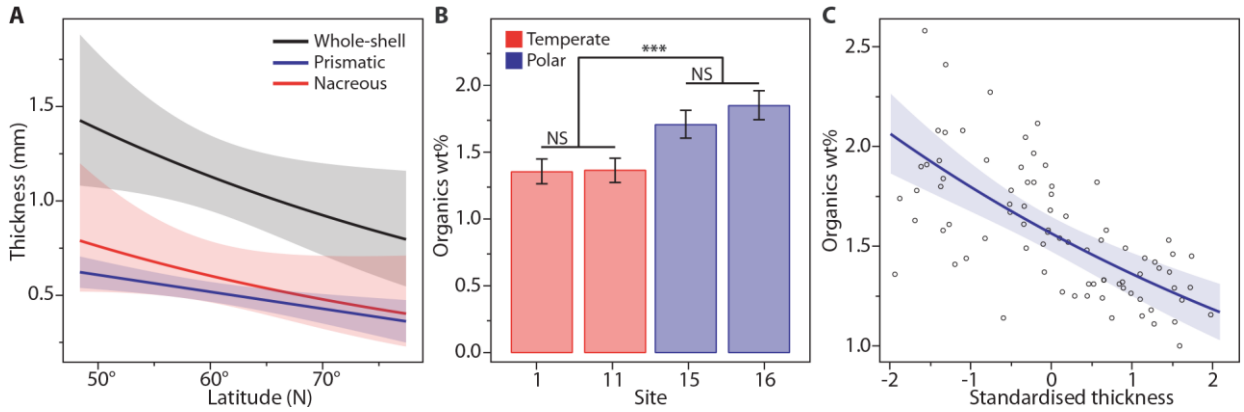

Fig. 2. Latitudinal patterns of shell thickness, organic content and calcification. (**A**) Relationships between the thickness of whole-shell (black), prismatic (blue) and nacreous (red) layers and latitude. Whole-shell thickness decreased poleward (95% CI = -0.36 to -0.01, cR^2 = 0.81). The prismatic layer was significantly related to latitude (95% CI = 4.70

673 to 5.73, $cR^2 = 0.72$). Predicted values (continuous lines) and confidence intervals (shaded
674 areas) were estimated for mussels of mean shell length (47.42 mm). Parameters'
675 significance is determined when the bootstrapped 95% CI does not include zero. (**B**)
676 Variations in organic content among shells from temperate (sites 1, 11, white bars) and
677 polar (sites 15, 16, grey bars) climates. Pair-wise contrasts indicated significantly higher
678 proportions of organics in high-latitude than low-latitude specimens [mean difference =
679 0.44%; $z = 8.27$, $P < 0.0001$ (***), $pseudoR^2 = 0.49$], in addition to non-significant
680 differences (NS) among temperate (mean difference = 0.002%; $z = 0.12$, $P = 0.91$) and
681 polar (mean difference = 0.13%, $z = 1.86$, $P = 0.063$) populations. (**C**) Relationship
682 between the proportion of organics and standardised thickness of the prismatic [mean (SD)
683 = 529 µm (174)] (sites 1, 7, 10 and 11), indicating a negative association between layer
684 thickness and calcification level ($z = -7.10$, $P < 0.0001$, $pseudoR^2 = 0.40$).
685

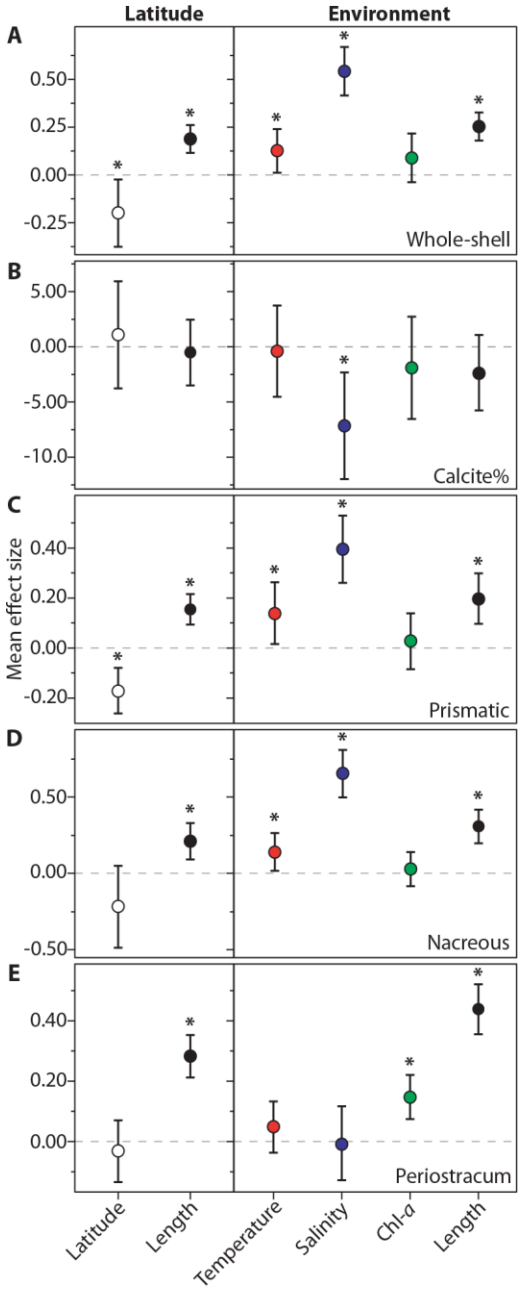

686

687 **Fig. 3. Mean effect size of predictors on *Mytilus* shell measurements.** Effect sizes were
688 estimated from individual latitudinal (left panels) and environmental (right panels)
689 GLMMs. Mean effect sizes and direction of impacts of latitude (white), shell length
690 (black), sea surface temperature (red), salinity (blue) and Chl-*a* concentration (green) on
691 layer ln-thickness (µm) measurements and calcite% are reported: (**A**) whole-shell, (**B**)
692 calcite%, (**C**) prismatic layer, (**D**) nacreous layer and (**E**) periostracum. Note the different

scales on the y-axis to highlight variations among layers. Significance of regression parameters is determined when the bootstrapped 95% CI (error bars) does not cross zero (* denotes a significant difference from zero).

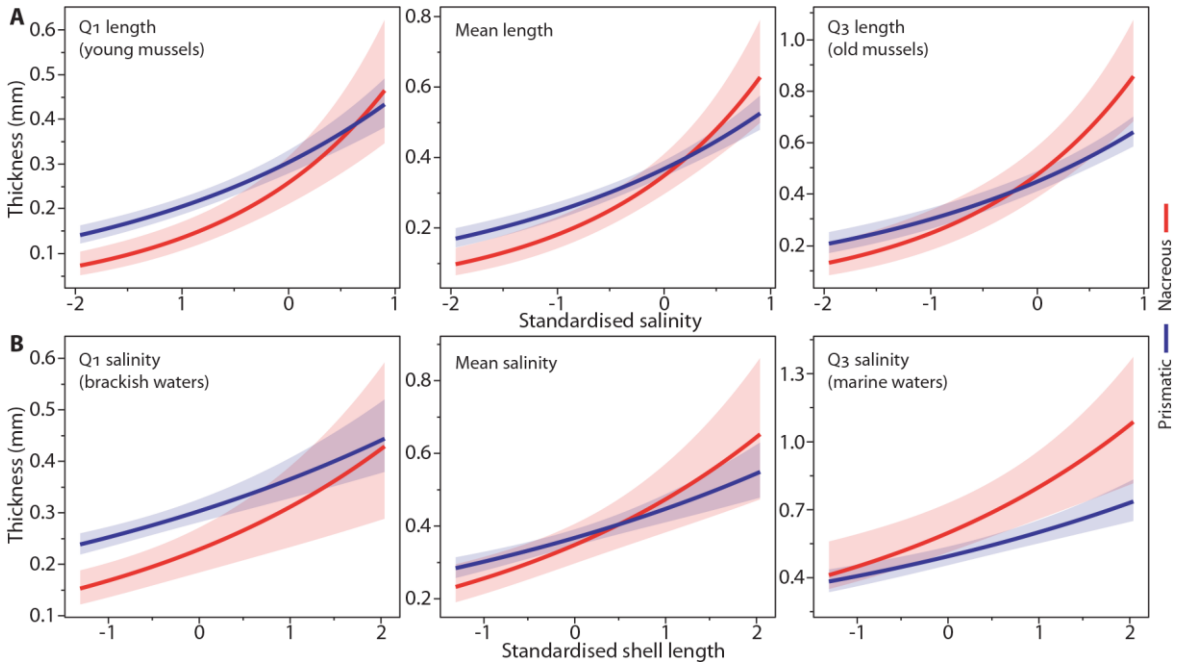

Fig. 4. Environmental influence on shell production and composition. Predicted relationships between thickness of prismatic (blue) and nacreous (red) layers, and standardised salinity [mean (SD) = 25.52 psu (10.29)], shell length [mean (SD) = 47.42 mm (16.20)] and their interactions. (**A**) Shell thickness is modelled as a function of salinity for the 1st quartile (Q_1 = 31.50 mm), mean value (47.42 mm) and 3rd quartile (Q_3 = 63.90 mm) of the shell lengths sampled. For medium-sized mussels, we detected a decreasing proportion of the calcitic component with increasing salinity and the deposition of relatively thicker aragonitic layers at salinities > 27.67 psu. (**B**) Thickness is modelled as a function of length for the 1st quartile (Q_1 = 18.92 psu), mean value (25.52 psu) and 3rd quartile (Q_3 = 33.13 psu) of salinity. At mean salinity, we detected an inversion of the relative layers' thickness

for shell length > 55.30 mm. Across the entire range of shell lengths, the model predicts formation of calcite- and nacreous-dominated shells under low- and high-salinities, respectively. Mean values (continuous lines) and confidence intervals (shaded areas) are predicted controlling for temperature (13.03°C) and Chl-*a* (2.48 mg m^{-3}).

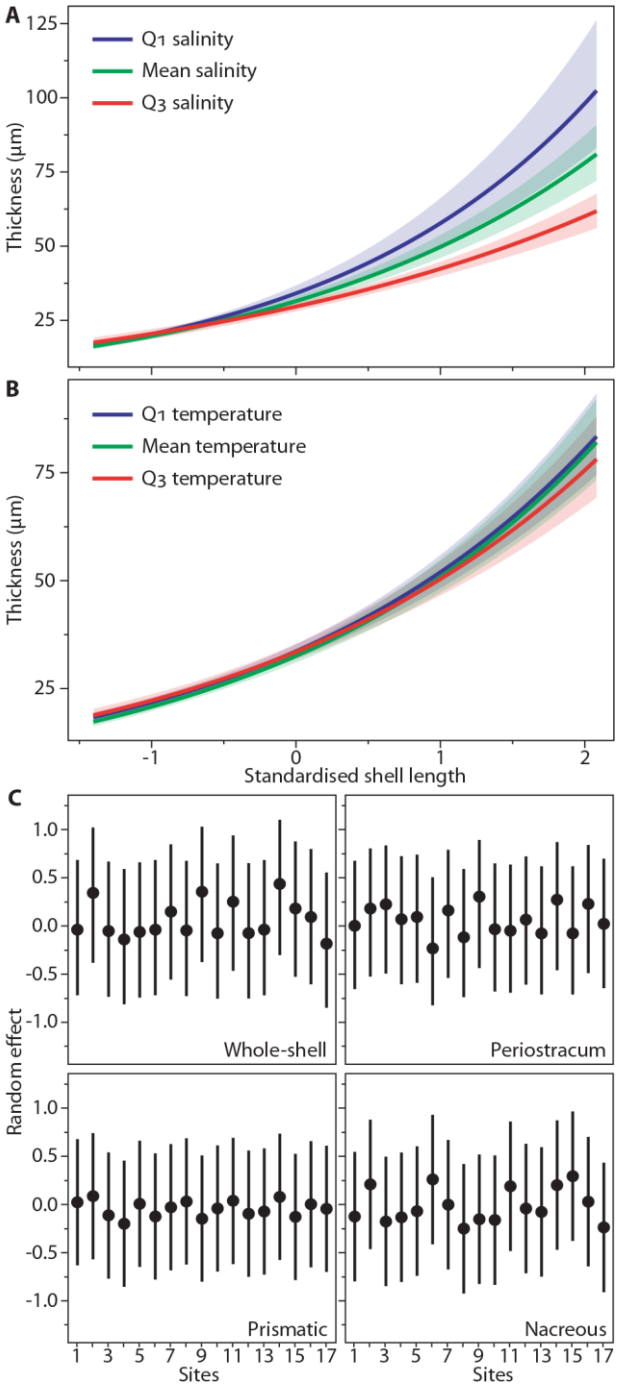

713

714 **Fig. 5. Periostracum plasticity and among-site shell variation.** Interacting effects of salinity,

715 temperature and shell length on shell periostracum. (**A**) Periostracum thickness is

716 modelled as a function of shell length [mean (SD) = 47.42 mm (16.20)] for the 1st

717 quartile (Q_1 = 18.92 psu, blue line), mean (25.52 psu, black line) and 3rd quartile (Q_3 =
718 33.13 psu, red line) of water salinity. Predicted values (continuous lines) and confidence
719 intervals (shaded areas) indicate higher rates of exponential periostracal thickening with
720 decreasing salinity. Smaller individuals (shell length < 48.38 mm) were characterized by
721 non-significant thickness differences under different salinity regimes. (**B**) Thickness is
722 modelled for the 1st quartile (Q_1 = 12.89°C, blue line), mean (13.03°C, black line) and
723 3rd quartile (Q_3 = 15.51°C, red line) of water temperature. Predicted values indicate a
724 marginal influence of temperature on periostracal thickening. (**C**) GLMMs' conditional
725 modes (filled circles) and variances (continuous lines) of the random effect estimated for
726 individual shell layers. Modes represent the difference between the average predicted
727 response (layer thickness) for a given set of fixed-effects values (mean environmental
728 covariates and shell length) and the response predicted at a particular site. These indicate
729 no detectable residual effect of species (*Mytilus edulis* or *M. trossulus*) and level of
730 hybridization on shell thickness for each site.
731
732 **Table 1. Environmental GLMMs summary.** Estimated statistics and bootstrapped 95% CIs for
733 regression parameters are reported for the modelled relationships between individual
734 shell thickness measurements and standardised covariates. For the summary of model in
735 equation (1), the prismatic layer, Layer(Pr), is used as the reference level, (Intercept).
736 (Parameters' significance is determined when the 95% CI does not include zero).

	Estimate	SE	95% CI	*t*-value	*P*-value (approximate)
Whole-shell*					
(Intercept)	6.617	0.051	6.517; 6.717	128.71	<0.0001

Temperature	0.156	0.054	0.014; 0.240	2.89	0.013
Salinity	0.525	0.060	0.411; 0.672	8.69	<0.0001
Chl-*a*	0.074	0.054	-0.042; 0.216	1.37	0.20
Length	0.248	0.037	0.181; 0.327	6.44	<0.0001
Prismatic (Pr) & nacreous (Na)[†]					
(Intercept)	5.907	0.031	5.774; 6.036	188.31	<0.0001
Temperature	0.138	0.033	0.013; 0.260	4.17	0.0011
Salinity	0.396	0.039	0.264; 0.531	10.22	<0.0001
Chl-*a*	0.028	0.033	-0.087; 0.139	0.86	0.41
Length	0.197	0.031	0.096; 0.297	6.39	<0.0001
Layer(Na)	-0.054	0.078	-0.247; 0.134	-0.70	0.49
Salinity × Layer(Na)	0.259	0.088	0.065; 0.443	2.95	0.0033
Length × Layer(Na)	0.111	0.067	-0.036; 0.258	1.66	0.096
Periostracum[‡]					
(Intercept)	3.500	0.048	3.406; 3.596	71.03	<0.0001
Temperature	0.049	0.043	-0.036; 0.134	1.12	0.28
Salinity	-0.009	0.061	-0.131; 0.111	-0.14	0.89
Chl-*a*	0.147	0.038	0.071; 0.221	3.88	0.0020
Length	0.439	0.041	0.357; 0.522	10.25	<0.0001
Temperature × Length	-0.064	0.035	-0.135; 0.006	-1.77	0.082
Salinity × Length	-0.151	0.061	-0.271; -0.029	-2.38	0.020

737 [*] Whole-shell, the random intercept was normally distributed with mean of 0 and variance 0.209^2.

738 [†] Prismatic and nacreous layer, the random intercepts were normally distributed with mean 0, and

739 variances 0.123^2 and 0.310^2, respectively.

740 [‡] Periostracum, the random intercept was normally distributed with mean 0 and variance 0.130^2.

741

742 # SUPPLEMENTARY MATERIALS

743

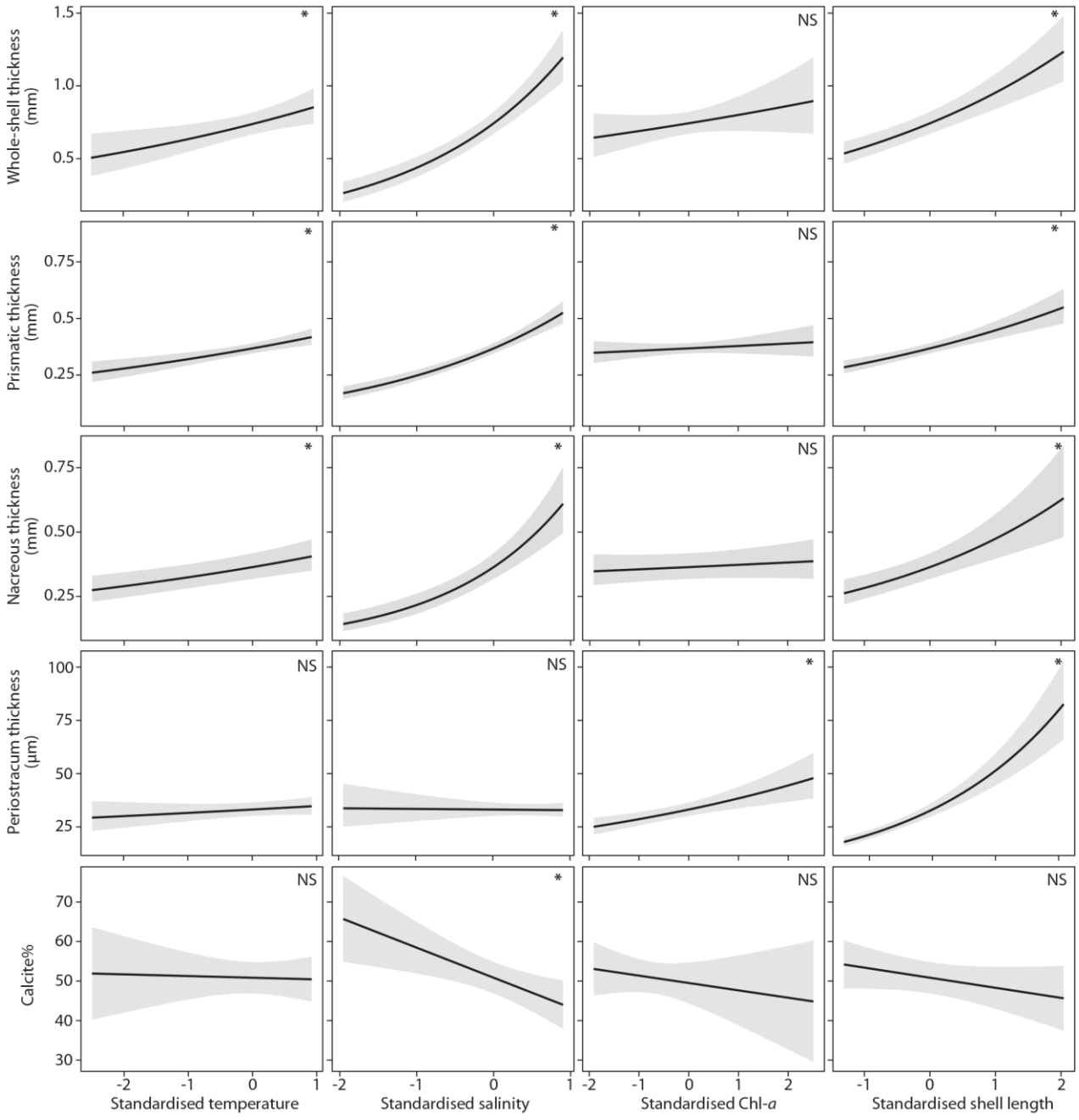

744

745 **fig. S1. Relationships between shell layers and modelled predictors.** Predicted relationships

746 between the whole-shell, prismatic layer, nacreous layer, periostracum thickness and the

747 calcite% with standardised water temperature [mean (SD) = 13.03°C (4.32)], salinity [mean (SD)

= 25.52 psu (10.29)], Chl-*a* concentration [mean (SD) = 2.48 mg m^{-3} (1.41)], and shell length [mean (SD) = 47.42 mm (16.20)]. Predicted values (continuous lines) and confidence intervals (shaded areas) across the range of each predictor were estimated controlling statistically for the other covariates (mean values). (NS $P > 0.05$, * $P < 0.05$)

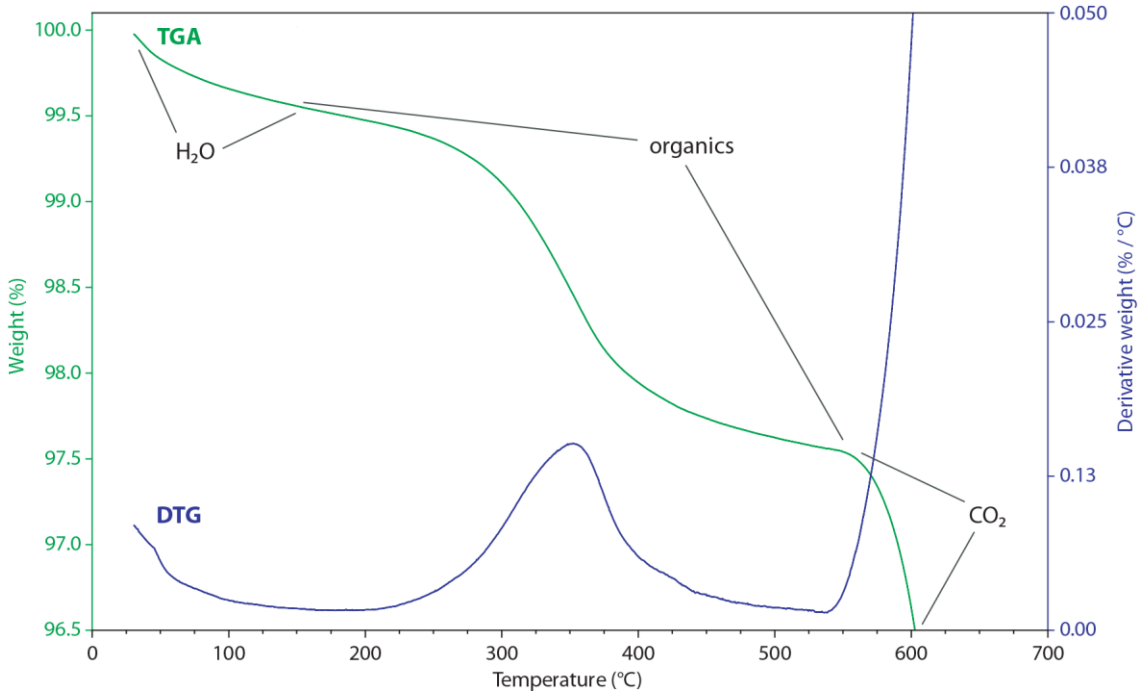

fig. S2. Example of Thermogravimetric Analysis (TGA) and Derivative Thermogravimetry (DTG). The TGA curve (green) represents the weight changes with increasing treatment temperature for the prismatic layer of *Mytilus edulis*. The sample was exposed to a constant heating, from ~25°C to 700°C at a linear rate of 10°C min^{-1}. Three known regions of weight loss with increasing temperature are highlighted (*42*): i) the evaporation of physically adsorbed water at 30-150°C, ii) the degradation of organics at 150-550 °C, and iii) the rapid decomposition of calcium carbonate ($CaCO_3$) into calcium oxide (CaO) and carbon dioxide (CO_2) starting at ~550°C. The DTG line (blue) represents the derivative of the thermal curve and shows the rate of

762 weight loss during heating. The peak indicates the temperature at which the organic mass loss
763 was fastest.

764

765 **table S1. Latitudinal GLMMs summary.** Estimated statistics and bootstrapped 95% CI for
766 regression parameters are reported for the modelled relationships between individual shell
767 measurements, standardised latitude and shell length.

Measurement	Fixed effects	Estimate	SE	95%CI	*t*-value	*P*-value (approximate)	Random effects	SD
Whole-shell	(Intercept)	7.036	0.089	6.863; 7.210	78.89	<0.0001	Site	0.293
	Latitude	-0.188	0.089	-0.316; -0.011	-2.10	0.067	Residuals	0.192
	Length	0.188	0.036	0.115; 0.259	5.18	<0.0001		
Prismatic	(Intercept)	6.211	0.267	6.118; 6.302	133.06	<0.0001	Site	0.867
	Latitude	-0.839	0.268	-1.373; -0.305	-3.13	0.013	Residuals	0.906
	Length	-0.786	0.155	0.478; 1.106	4.83	<0.0001		
Nacreous	(Intercept)	6.410	0.135	6.148; 6.674	47.63	<0.0001	Site	0.442
	Latitude	-0.217	0.135	-0.480; 0.050	-1.61	0.14	Residuals	0.321
	Length	0.210	0.060	0.089; 0.332	3.39	0.00088		
Periostracum	(Intercept)	3.709	0.053	3.605; 3.814	70.02	<0.0001	Site	0.170
	Latitude	-0.031	0.053	-0.136; 0.073	-0.59	0.58	Residuals	0.224
	Length	0.283	0.035	0.213; 0.353	7.65	<0.0001		
Calcite%	(Intercept)	45.255	2.476	40.327; 50.134	18.28	<0.0001	Site	8.019
	Latitude	1.097	2.484	-3.718; 6.011	0.44	0.67	Residuals	8.829
	Length	-0.510	1.486	-3.444; 2.515	-0.33	0.75		

768 **table S2. Environmental GLMMs summary.** Estimated statistics and bootstrapped 95% CI for
769 regression parameters are reported for the modelled relationships between individual shell
770 measurements, standardised environmental covariates and shell length.

Measurement	Fixed effects	Estimate	SE	95%CI	*t*-value	*P*-value (approximate)	Random effects	SD
Whole-shell	(Intercept)	6.617	0.051	6.517; 6.717	128.62	<0.0001	Site	0.209

	Temperature	0.156	0.054	0.014; 0.240	2.89	0.013	Residual	0.188
	Salinity	0.525	0.060	0.411; 0.672	8.69	<0.0001		
	Chl-*a*	0.074	0.054	-0.042; 0.216	1.37	0.20		
	Length	0.248	0.037	0.181; 0.327	6.44	<0.0001		
Prismatic (Pr) and nacreous (Na)	(Intercept)	5.907	0.031	5.774; 6.036	188.31	<0.0001	Site (Pr)	0.123
	Temperature	0.138	0.033	0.013; 0.260	4.17	0.0011	Site (Na)	0.310
	Salinity	0.396	0.039	0.264; 0.531	10.22	<0.0001	Residual	0.198
	Chl-*a*	0.028	0.033	-0.087; 0.139	0.86	0.41		
	Length	0.197	0.031	0.096; 0.297	6.39	<0.0001		
	Layer(Na)	-0.054	0.078	-0.247; 0.134	-0.70	0.49		
	Salinity × Layer(Na)	0.259	0.088	0.065; 0.443	2.95	0.0033		
	Length × Layer(Na)	0.111	0.067	-0.036; 0.258	1.66	0.096		
Periostracum	(Intercept)	3.500	0.048	3.406; 3.596	71.03	<0.0001	Site	0.130
	Temperature	0.049	0.043	-0.036;0.134	1.12	0.28	Residual	0.230
	Salinity	-0.009	0.061	-0.131;0.111	-0.14	0.89		
	Chl-*a*	0.147	0.038	0.071;0.221	3.88	0.002		
	Length	0.439	0.041	0.357; 0.522	10.25	<0.0001		
	Temperature × Length	-0.064	0.035	-0.135; 0.006	-1.77	0.082		
	Salintiy × Length	-0.151	0.061	-0.271; -0.029	-2.38	0.020		
Calcite%	(Intercept)	51.092	1.903	47.338; 54.927	26.84	<0.0001	Site	7.605
	Temperature	-4.003	2.112	-4.508; 3.791	-0.19	0.85	Residual	9.656
	Salinity	-7.163	2.476	-12.025; -2.382	-2.87	0.012		
	Chl-*a*	-1.908	2.392	-6.662; 2.764	-0.80	0.44		
	Length	-2.404	1.690	-5.807; 1.071	-1.367	0.18		

771

772 **table S3. Provenience and taxonomic status of the *Mytilus* populations used for the study.**
773 For each sampling site (site codes as in Fig. 1C), geographic location, samples size (*N*), site
774 coordinates (longitude and latitude), genotypic status [proportion of *Mytilus edulis* (Me), *M.*
775 *trossulus* (Mt), *M. galloprovincialis* (Mg) and hybrids] and reference and/or previous use of the
776 studied populations are reported.

Site	Location	*N*	Longitude	Latitude	Status of mussels	Reference to taxonomic status of populations and/or previously published use of the shells
1	Brest (France)	25	4.369375°W	48.338°N	96%Me, 4%Me×Mg	Kijewski *et al.* (*43*); Bierne *et al.* (*44*)
2	Exmouth (England, UK)	26	3.429111°W	50.622°N	Me	Hilbish *et al.* (*45*); Annual monitoring 2015
3	Oostende (Belgium)	25	2.904333°E	51.23039°N	Me	Kijewski *et al.* (*43*, *46*)
4	Texel (Netherlands)	25	4.796167°E	53.00536°N	94%Me, 6%Me×Mg	Kijewski *et al.* (*43*, *46*)
5	Usedom (Germany)	25	14.01103°E	54.05561°N	37%Me, 10%Mt, 53%Me×Mt	Stuckas *et al.* (*47*); Kijewski *et al.* (*48*)
6	Kiel (Germany)	25	10.14889°E	54.32919°N	68%Me, 32%Me×Mt	Stuckas *et al.* (*47*, *49*); Breusing (*50*)
7	Ahrenshoop (Germany)	25	12.42694°E	54.38686°N	80%Me, 20%Me×Mt	Stuckas *et al.* (*47*, *49*); Kijewski *et al.* (*43*)
8	Sylt (Germany)	25	8.435944°E	55.02556°N	Me	Stuckas *et al.* (*47*, *49*); Breusing (*50*); Väinölä & Strelkov (*51*); Bierne (*44*)
9	Kerteminde (Denmark)	25	10.66797°E	55.45125°N	57%Me, 5%Mt, 38%Me×Mt	Stuckas *et al.* (*47*); Kijewski *et al.* (*48*)

10	Tarbet (Scotland, UK)	25	5.411333°W	55.86556°N	Me	Yarra *et al.* (*52*)
11	St. Andrews (Scotland, UK)	25	2.781472°W	56.33961°N	Me	Tyler-Walters *et al.* (*53*); Annual MPA monitoring (JCNN, SNH)
12	Kristineberg (Sweden)	24	11.42208°E	58.2105°N	94%Me, 6%Me×Mt	Stuckas *et al.* (*47*, *49*); Brooks & Farmed (*54*); Breusing (*50*); Kijewski *et al.* (*43*); Väinölä & Strelkov (*51*)
13	Nynäshamn (Sweden)	25	17.92928°E	58.87736°N	Mt	Stuckas *et al.* (*47*, *49*); Breusing (*50*); Väinölä & Strelkov (*51*); Kijewski *et al.* (*43*)
14	Trondheim (Norway)	25	10.44789°E	63.45719°N	70%Me, 5%Mt, 25%Me×Mt, 5%Me×Mg	Brooks & Farmed (*54*); Väinölä & Strelkov (*51*)
15	Tromsø (Norway)	24	56.10281°W	70.07467°N	Me	Mathiesen *et al.* (*55*); Brooks & Farmed (*54*); Väinölä & Strelkov (*51*)
16	Upernavik (Greenland)	25	56.10281°W	72.79389°N	33% Me, 51%Mt, 14%Me×Mt	Mathiesen *et al.* (*55*)
17	Qaanaaq (Greenland)	25	69.24031°W	77.465°N	Mt	Mathiesen *et al.* (*55*)

777 **table S4. Environmental covariates.** Summary statistics (mean value and SD) of environmental

778 conditions at each study site. Site codes as in Fig. 1C.

Site	Temperature (SD) (°C)	Salinity (SD) (psu)	Chl-*a* (SD) (mg m^{-3})
1	17.01 (1.94)	34.79 (0.33)	2.16 (1.00)
2	15.08 (1.92)	34.70 (0.39)	2.14 (0.98)
3	16.33 (2.55)	32.70 (1.92)	1.76 (0.75)
4	16.19 (2.82)	30.20 (2.28)	1.84 (0.93)
5	15.59 (3.67)	5.39 (1.45)	7.62 (3.02)
6	15.46 (3.11)	13.77 (2.54)	5.34 (7.10)
7	15.39 (3.34)	9.09 (1.24)	2.16 (1.25)
8	15.51 (3.10)	29.34 (1.14)	1.29 (0.70)
9	15.08 (3.09)	18.92 (3.57)	2.83 (1.40)
10	13.43 (2.15)	33.51 (0.49)	3.95 (3.72)
11	12.89 (2.14)	33.13 (0.57)	2.36 (1.12)
12	15.30 (3.39)	24.90 (2.20)	1.21 (0.59)
13	12.95 (4.28)	5.92 (0.45)	1.94 (1.07)
14	10.82 (2.39)	29.47 (1.35)	3.18 (2.55)
15	9.42 (2.49)	33.67 (0.37)	0.94 (0.81)
16	2.70 (2.74)	32.60 (0.53)	0.58 (0.54)
17	2.23 (3.46)	31.64 (0.97)	0.75 (0.61)

779

780 **table S5. List of R packages.** Packages and version used with the R software (v3.4.1) (*56*) for
781 data exploration, statistical analysis and graphing.

Package	Complete name	Version	Year	Author	Use
betareg	Beta Regression	3.1	2016	Cribari-Neto & Zeileis (*57*)	Beta regression (GLM with beta distribution)
car	Companion to Applied Regression	2.1-5	2017	Fox et al. (*58*)	Type III ANOVA table
ggplot2	Create Elegant Data Visualisations Using the Grammar of Graphics	2.2.1	2016	Wickham et al. (*59*)	Graphing
lme4	Linear Mixed-Effects Models using 'Eigen' and S4	1.1-13	2017	Bates et al. (*60*)	Mixed-effect models (GLMMs)
lmeresampler	Bootstrap Methods for Nested Linear Mixed-Effects Models	0.1.0	2016	Loy & Steele (*61*)	Parametric bootstrap for nlme model
lmerTest	Tests in Linear Mixed Effects Models	2.0-33	2016	Kuznetsova et al. (*62*)	Wald approximated confidence intervals
MuMIn	Multi-Model Inference	1.40.0	2017	Barton (*63*)	Pseudo-R-squared for Generalized Mixed-Effect models

nlme	Linear and Nonlinear Mixed Effects Models	3.1-131	2017	Pinheiro et al. (*64*)	Mixed-effect models (GLMMs), variance structure (GLS), spatial correlation
pbkrtest	Parametric Bootstrap and Kenward Roger Based Methods for Mixed Model Comparison	0.4-7	2017	Halekoh & Højsgaard (*65*)	Kenward-Roger approximations for degrees of freedom and parametric bootstrap for model comparisons
RLRsim	Exact (Restricted) Likelihood Ratio Tests for Mixed and Additive Models	3.1-3	2016	Scheipl et al. (*66*)	random effect simulation, exact restricted likelihood ratio tests simulations

SUPPLEMENTARY MATERIALS AND METHODS

Protocol for Thermal Gravimetric Analyses. Thermogravimetric Analyses (TGA) are reported following the guidelines made by the Committee on Standardisation of the International Confederation for Thermal Analysis and Calorimetry (ICTAC) and appeared in standards as ASTM E 472 (1991) (*67*, *68*).

A. Properties of the sample

1. *Source of material and identification*
    - Shell of wild Atlantic blue mussel (*Mytilus edulis*).
    - Prismatic layer composed of calcium carbonate ($CaCO_3$, calcite), variable amount of organics (~1-2%) and trace elements, such as quartzite (SiO_2) and magnesium (Mg).

794 2. *Sample history*

795 • Shells were cleaned, raised with mill-Q water, dried at room temperature for
796 seven days.

797 • The periostracum was removed by sanding and a tile of prismatic layer isolated (8
798 x 5 mm) with a Dremel rotary tool (Dremel 300/395RD MultiPro, Racine,
799 Wisconsin, USA).

800 • Samples were cleaned in an ultrasonic bath (Ultrasonic Cleaner CD-4800,
801 Practical Systems Inc., Odessa, FL, USA) with mill-Q water, air-dried and
802 powdered with an agate mortar.

803 • Additional, oven drying (30°C for 24h, convection oven) to remove residual pre-
804 treatment water.

805 3. *Physical properties*

806 • Fine grade powder.

807 **B. Experimental conditions**

808 1. *Apparatus used*

809 • Thermogravimetric Analyser: TGA Q500, TA instrument (New Castle, DE, USA)
810 Q series.

811 2. *Thermal treatment*

812 • Initial temperature, ~25°C (room temperature).

813 • Final temperature, 700°C.

814 • Linear rate of heating, 10°C min^{-1}.

815 3. *Sample atmosphere*

816 • Dynamic (flowing) atmosphere.

- Flow rate for balance 40 ml min^{-1} and for sample 60ml min^{-1}.
- Gas composition: nitrogen, "white spot".

4. *Sample holder*

- Platinum crucible, cylindrical: diameter 10 mm and height 1.5 mm.
- Sample was tipped and spread to cover the bottom of the crucible.

5. *Sample mass*

- 10 mg of powder were weighted on a separate micro-balance (Ultramicro 4504 MP8, Sartorius, Göttingen; readability 0.1 µg).

C. Data acquisition and manipulation methods

1. *Software version*

- Universal Analysis 2000, version 4.5A, TA instrument (New Castle, DE, USA).

SUPPLEMENTARY DATA

Environmental datasets. List of the datasets used for the calculation of mean annual values of environmental descriptors. Water temperature, salinity and chlorophyll-a concentrations were expressed as mean values (May - October) averaged over the 6-year period 2009 - 2014. This study has been conducted using the Copernicus Marine Service Products: COPERNICUS - Marine Environment Monitoring System (http://marine.copernicus.eu/).

DATASET #1

Product identifier	**GLOBAL_ANALYSIS_FORECAST_PHY_001_024**
Link (last accessed on 26-02-2018)	http://marine.copernicus.eu/services-portfolio/access-to-products/?option=com_csw&view=details&product_id=GLOBAL_ANALYSIS_FORECAST_PHY_001_024

Short description	The Operational Mercator global Ocean analysis and forecast system at 1/12 degree is providing 7 days of 3D global ocean forecasts updated daily and ocean analysis updated weekly. The time series start on January 1st 2013 and is aggregated in time in order to reach a two full years' time series sliding window. This product includes daily mean files of temperature, salinity, currents, sea level and ice parameters from the top to the bottom of the Ocean over the Global Ocean. It also includes 2-hourly mean surface fields for temperature, currents and sea level.
Spatial resolution	0.08 degree
Vertical coverage	from -5500.0 m to 0.0 m
Temporal resolution	Daily mean, hourly mean
Update frequency	Daily
Production unit	GLO-MERCATOR-TOULOUSE-FR

DATASET #2

Product identifier	**NORTHWESTSHELF_ANALYSIS_FORECAST_BIO_004_002_b**
Link (last accessed on 26-02-2018)	http://marine.copernicus.eu/services-portfolio/access-to-products/?option=com_csw&view=details&product_id=NORTHWESTSHELF_ANALYSIS_FORECAST_BIO_004_002_b

Short description	The Forecasting Ocean Assimilation Model, Atlantic Margin model (FOAM AMM7) is a coupled hydrodynamic-ecosystem model, nested in a series of one-way nests to the Met Office global ocean model. The hydrodynamics are supplied by the Nucleus for European Modelling of the Ocean (NEMO) with the 3DVar NEMOVAR system used for the assimilation of sea surface temperature data. This is coupled to the European Regional Seas Ecosystem Model (ERSEM), developed at Plymouth Marine Laboratory (PML). ERSEM based models have been used operationally to forecast biogeochemistry in the region for a number of years.
Spatial resolution	0.11 x 0.7 degree
Vertical coverage	from -5000 m to 0 m
Temporal resolution	Daily mean
Update frequency	Daily
Production unit	NWS-METOFFICE-EXETER-UK

DATASET #3

Product identifier	**GLOBAL_REANALYSIS_BIO_001_018**
Link (last accessed on 26-02-2018)	http://marine.copernicus.eu/services-portfolio/access-to-products/?option=com_csw&view=details&product_id=GLOBAL_REANALYSIS_BIO_001_018

Short description	Biogeochemistry simulation over period 1998 - 2015. Outputs are delivered as monthly mean files with .netcdf format (CF/COARDS 1.5 convention) on the native tri-polar grid (ORCA025) at ¼° resolution with 75 vertical levels. This simulation is based on the PISCES biogeochemical model. It is forced offline at a daily frequency by the equivalent of the GLOBAL-REANALYSIS-PHYS-001-009 physics product.
Spatial resolution	0.11 degree
Vertical coverage	from -5500.0 m to 0.0 m
Temporal resolution	Daily mean
Update frequency	Daily
Production unit	GLO-MERCATOR-TOULOUSE-FR

DATASET #3

Product identifier	**NORTHWESTSHELF_ANALYSIS_FORECAST_BIO_004_002_b**
Link (last accessed on 26-02-2018)	http://marine.copernicus.eu/services-portfolio/access-to-products/?option=com_csw&view=details&product_id=NORTHWESTSHELF_ANALYSIS_FORECAST_BIO_004_002_b

Short description	The Forecasting Ocean Assimilation Model, Atlantic Margin model (FOAM AMM7) is a coupled hydrodynamic-ecosystem model, nested in a series of one-way nests to the Met Office global ocean model. The hydrodynamics are supplied by the Nucleus for European Modelling of the Ocean (NEMO) with the 3DVar NEMOVAR system used for the assimilation of sea surface temperature data. This is coupled to the European Regional Seas Ecosystem Model (ERSEM), developed at Plymouth Marine Laboratory (PML). ERSEM based models have been used operationally to forecast biogeochemistry in the region for a number of years.
Spatial resolution	0.11 x 0.7 degree
Vertical coverage	from -5000 m to 0 m
Temporal resolution	Daily mean
Update frequency	Daily
Production unit	NWS-METOFFICE-EXETER-UK

DATASET #4

Product identifier	**NORTHWESTSHELF_REANALYSIS_BIO_004_011**
Link (last accessed on 26-02-2018)	http://marine.copernicus.eu/services-portfolio/access-to products/?option=com_csw&view=details&product_id=NORTHWESTSHELF_REANALYSIS_BIO_004_011

Short description	This is a hydrodynamic model of the North West European shelf forced at the surface by ERA-interim winds, atmospheric temperature, and precipitation fluxes. Horizontal boundary conditions were provided by the NOC global reanalysis prior to 1989 and by the GloSea reanalysis thereafter. Boundary conditions in the Baltic Sea came from the IOM-GETM model and CMEMS_BALTICSEA_ANALYSIS_FORECAST_ PHYS_003_006. E-Hype data were used for river inputs. Hydrodynamic calculations were performed by the Nucleus for European Modelling of the Ocean (NEMO) system, while the 3DVar NEMOVAR system was used for the assimilation of sea surface temperature data. Physical outputs are provided both as monthly means and as daily 25 hours, edited, averages. The reanalysis was conducted in four sections.
Spatial resolution	0.11 x 0.7 degree
Vertical coverage	from -5000.0 m to 0.0 m
Temporal resolution	Daily mean
Update frequency	Daily
Production unit	NWS-METOFFICE-EXETER-UK

DATASET #5

Product identifier	**BALTICSEA_ANALYSIS_FORECAST_PHYS_003_006**
Link (last accessed on 26-02-2018)	http://marine.copernicus.eu/services-portfolio/access-to-products/?option=com_csw&view=details&product_id=BALTICSEA_ANALYSIS_FORECAST_PHY_003_006
Short description	This Baltic Sea physical model product provides forecasts for the physical conditions in the Baltic Sea. The Baltic forecast is updated twice daily providing a new two days forecast with hourly data for sea level variations, ice concentration and thickness at the surface, and temperature, salinity and horizontal velocities for the 3D field. The product is based on the 3D ocean model code HBM developed within the Baltic ocean community.
Spatial resolution	2 km
Vertical coverage	from -5500.0 m to 0.0 m
Temporal resolution	Daily mean, hourly mean
Update frequency	Daily
Production unit	GLO-MERCATOR-TOULOUSE-FR

DATASET #6

Product identifier	**BALTICSEA_ANALYSIS_FORECAST_BIO_003_007**

Link (last accessed on 26-02-2018)	http://marine.copernicus.eu/services-portfolio/access-to-products/?option=com_csw&view=details&product_id=BALTICSEA_ANALYSIS_FORECAST_BIO_003_007
Short description	This Baltic Sea biogeochemical model product provides forecasts for the biogeochemical conditions in the Baltic Sea. The Baltic forecast is updated twice daily providing a new two days forecast with hourly data for the parameters dissolved oxygen, nitrate, phosphate, chl-a. The product is produced by the biogeochemical model ERGOM one way coupled to the Baltic 3D ocean model HBM, which provides the CMEMS Baltic physical ocean forecast product.
Spatial resolution	2 km
Vertical coverage	from -400 m to 0 m
Temporal resolution	Daily mean, hourly instantaneous
Update frequency	Daily
Production unit	BAL-DMI-COPENHAGEN-DK